JNeurosci
THE JOURNAL OF NEUROSCIENCE

**Research Articles | Systems/Circuits**

# A cortical mechanism linking saliency detection and motor reactivity in rhesus monkeys

https://doi.org/10.1523/JNEUROSCI.0422-23.2023

Received: 8 March 2023
Revised: 5 October 2023
Accepted: 10 October 2023

# A cortical mechanism linking saliency detection and motor reactivity in rhesus monkeys

Giacomo Novembre[1], Irene Lacal[2,3], Diego Benusiglio[4,5], Eros Quarta[2], Andrea Schito[2], Stefano Grasso[2], Ludovica Caratelli[2], Roberto Caminiti[2,4], Alexandra Battaglia Mayer[2,*], Gian Domenico Iannetti[4,6,*]

[1]Neuroscience of Perception & Action Lab, Italian Institute of Technology, Rome, Italy

[2]Department of Physiology and Pharmacology, University of Rome, Sapienza, Italy

[3]Cognitive Neuroscience Laboratory, German Primate Center – Leibniz-Institute for Primate Research, Germany

[4]Neuroscience and Behaviour Laboratory, Italian Institute of Technology, Rome, Italy

[5]European Molecular Biology Laboratory (EMBL), Epigenetics and Neurobiology Unit, Rome, Italy

[6]Department of Neuroscience, Physiology and Pharmacology, University College London (UCL), London, UK

*shared senior authorship

**Abbreviated title**: Saliency detection in rhesus monkeys

**Corresponding author**: Dr. Giacomo Novembre; Neuroscience of Perception & Action Lab. Viale Regina Elena 291, 00161 Rome, Italy; Phone: +39 06 49255199 Italian Institute of Technology (IIT). Email to Giacomo.novembre@iit.it

**Number of figures**: 7

**Number of words**: abstract (166), introduction (751), discussion (1451).

**Conflict of interest**: n/a

**Acknowledgments**: GN acknowledges the support of the European Research Council (Starting Grant MUSICOM). GDI acknowledges the support of the European Research Council (Consolidator Grant PAINSTRAT) and of The Wellcome Trust (COLL JLARAXR). ABM acknowledges the support of The Italian Ministry of Education (Grant. N. 201794KEER_002).

## Abstract

Sudden and surprising sensory events trigger neural processes that swiftly adjust behavior. To study the phylogenesis and the mechanism of this phenomenon, we trained two male rhesus monkeys to keep a cursor inside a visual target by exerting force on an isometric joystick. We examined the effect of surprising auditory stimuli on exerted force, scalp electroencephalographic (EEG) activity, and local field potentials (LFP) recorded from the dorso-lateral prefrontal cortex. Auditory stimuli elicited (1) a biphasic modulation of isometric force: a transient decrease followed by a corrective tonic increase, and (2) EEG and LFP deflections dominated by two large negative-positive waves (N70 and P130). The EEG potential was maximal at the scalp vertex, highly reminiscent of the human 'vertex potential'. Electrocortical potentials and force were tightly coupled: the P130 amplitude predicted the magnitude of the corrective force increase, particularly in the LFPs recorded from deep rather than superficial cortical layers. These results disclose a phylogenetically-preserved cortico-motor mechanism supporting adaptive behavior in response to salient sensory events.


## Significance Statement

Survival in the natural world depends on an animal's capacity to adapt ongoing behavior to unexpected events. To study the neural mechanisms underlying this capacity, we trained monkeys to apply constant force on a joystick while we recorded their brain activity from the scalp and, invasively, from the prefrontal cortex contralateral to the hand holding the joystick. Unexpected auditory stimuli elicited a biphasic force modulation: a transient reduction followed by a corrective adjustment. The same stimuli also elicited EEG and LFP responses, dominated by a biphasic wave that predicted the magnitude of the behavioral adjustment. These results

disclose a phylogenetically-preserved cortico-motor mechanism supporting adaptive behavior in response to unexpected events.

**Keywords:** Electroencephalography (EEG), local field potentials (LFP), event-related potentials (ERPs), monkey, saliency, force.

## Introduction

Survival in the natural world depends heavily on an animal's capacity to identify sudden threats or affordances, and to quickly adapt ongoing behavior accordingly, with none or scarce influence of volition. We recently referred to this as Reactive Adaptive Behavior (RAB): sudden sensory stimuli elicit swift involuntary behavioral responses that are, however, flexible on the basis of the current environmental context (Novembre and Iannetti 2021).

There are multiple examples of RAB in the literature. One is cortico-muscular resonance (CMR), which consists of a series of fast modulations of muscular activity in response to sudden and task-irrelevant sensory stimuli [(Novembre et al. 2018, 2019) see also (Somervail et al. 2021; Rangel et al. 2023)]. When humans exert a constant isometric force on a transducer held between the index finger and the thumb, such stimuli elicit an initial force decrease (*d1*, peaking ~100 ms post-stimulus) followed by two consecutive force increases (*i1*, peaking at ~250 ms; *i2*, starting ~300−350 ms and lasting for ~2 s). These force modulations are tightly coupled, both on a trial-by-trial basis and across-subjects, to the large EEG 'vertex potential' elicited by the same stimuli evoking the CMR (Bancaud et al. 1953; Walter 1964; Mouraux and Iannetti 2009; Novembre et al. 2018). EEG responses like the vertex potential, as well as other responses such as the mismatch negativity and the P300, are believed to capture the violation of an internal model of the sensory environment (Picton 1992; Näätänen et al. 2007; Luck 2014). As such, the coupling between such EEG responses – classically associated to sensory systems – and motor output is intriguing. It suggests that updating a model of the sensory environment might often and automatically trigger an action (or RAB), as it is indeed predicted by several models of saliency detection and orienting behavior (Sokolov 1963; Neumann 1990; Engbert and Kliegl 2003; Menon and Uddin 2010).

The CMR falls within the definition of RAB: it is elicited in an automatic and unconscious manner, i.e. participants are unaware of producing a response, yet the force modulations is enhanced when the eliciting stimulus has high behavioral relevance (Novembre and Iannetti 2021).

Thus the CMR, as well as RABs in general, are likely to be important for animal survival. As such, one would guess that these behavioral responses are well conserved phylogenetically. Yet, whether CMR is also observable in other species besides humans is unknown. Nevertheless, other RABs such as stimulus-locked responses (Corneil et al. 2004, 2008; Pruszynski et al. 2010; Goonetilleke et al. 2015), online motor corrections (Lee and Tatton 1975; Battaglia-Mayer et al. 2013, 2014; Scott 2016) or action stopping (Boehler et al. 2009; Schevernels et al. 2015; Wessel and Aron 2017; Giarrocco et al. 2021), exist in both humans and non-human primates, suggesting that CMR might also be observable in non-human primates.

Therefore, the first aim of the current study was to investigate whether the CMR is present in non-human primates. To do so, across two Experiments, we exploited a well-established behavioral task that requires rhesus monkeys (*Macaca mulatta*) to control the position of a cursor on a screen using a hand-held force-sensitive isometric joystick (Fig. 1a) (Ferrari-Toniolo et al. 2015; Satta et al. 2017). Animals were trained to hold the cursor inside a central target, an action that implied the production of a small, constant force, while isolated fast-rising and task-irrelevant auditory stimuli were presented in a minority of the trials (Beep Trials).

The second aim of this study was to investigate the neurophysiology of the CMR. In Experiment 1, based on the previous demonstration of a tight coupling between saliency-related vertex potentials and CMR in humans, we used 29 active electrodes to record

electroencephalographic (EEG) activity in awake monkeys performing the task described above (Fig. 1a,c). We examined event-related EEG potentials elicited by the salient stimuli and their relationship with the CMR. In Experiment 2 we repeated the above procedure recording intracortically local field potentials (LFP) from the right dorso-lateral prefrontal cortex (dlPFC, putatively Brodmann Area 9, BA9) – a cortical area that has been shown to be involved in hand force control in both human (Ehrsson et al. 2000; Vaillancourt et al. 2007) and non-human primates (Badoud et al. 2017). Notably, BA9 lesioning leads to a bilateral impairment of fine hand force control, leaving general motor behavior intact (Badoud et al. 2017). Furthermore, the LFP recordings allowed us to compare the effect of responses measured at different cortical depths. This latter notion might shed light upon the specific circuits through which BA9 might contribute to the CMR.

Figure 1 about here

## Materials and Methods

### *Animals and surgical procedures*

Two male rhesus monkeys (*Macaca mulatta*) participated to the experiments: Monkey M (9 years old, 9.1 Kg) and Monkey T (9 years old, 9.4 Kg). One headpost was mounted on the skull in each animal. In between experiment 1 (EEG) and 2 (LFP), a circular chamber (diameter = 18 mm) was implanted for intracranial recording. The chamber was placed on the right hemisphere, centered at stereotaxic coordinates A +35; L +6 (Monkey 1) and A +35; L +7 (Monkey 2), in both cases corresponding to dorso-lateral prefrontal cortex (specifically BA 9). During the surgical procedures, the animals were pre-anaesthetized with ketamine (10

mg/kg, i.m.) and then anaesthetized with a mix of Oxygen/Isoflurane (1-3% to effect). Skull implants were performed under aseptic conditions. After surgery, the animals were allowed to recover for at least 7 days, while being treated with antibiotic and pain relievers, according to veterinary prescriptions. All efforts were made to minimize animals' pain and distress. Animal care, housing and surgical procedures were in agreement with European (EU Directive 63-2010) and Italian (DL. 26/2014) laws on the use of non-human primates in scientific research.

*Experimental setup*

The experimental setup is illustrated in Fig. 1a. Each monkey was placed in a soundproof chamber, seating on a primate chair in front of a 40-inch monitor (100 Hz, 800-600 resolution, 32-bit color depth; monitor-eye distance: 150 cm). Each animal was trained to control a colored circular cursor by applying a hand force on an isometric joystick [consisting of a 1.5-6.5-cm metal cylinder mounted on top of a force transducer: FTS-Gamma (Calibration SI-32-2.5) ATI Industrial Automation, Apex NC]. The cursor [0.6 degrees of visual angle (DVA)] was displayed on a black screen. The force exerted on the transducer was sampled (at 1 kHz) on both the x- and y-axes, corresponding to hand force exerted towards the left/right (x axis) and towards/away from the animal's body (y axis) (Fig. 1a). Each animal faced the monitor from one out of two personalized primate chairs placed one next to the other. Consequently, Monkey M had the monitor slightly on its right side (approximately 30 degrees from the midline, i.e. at 1 o'clock) while Monkey T slightly on its left-side (approximately at 11 o'clock).

The force exerted on the transducer was used to control the position of the cursor on the monitor, so that a force of 20N applied on the y axis (away from the animal's body) was necessary to hold the cursor in the central target (Fig. 1). Sudden and unexpected auditory stimuli were produced using a beeper placed behind the monitor, ~160 cm away from the

monkey's head (Fig. 1a). Stimuli presentation and data sampling were controlled using the software package REX (Ferrari-Toniolo et al. 2019).

Both monkeys were required to use the left hand to perform the task, while the right arm was gently restrained. The joystick was controlled using the left hand because both monkeys appeared to prefer this configuration during the early stages of their training. We prevented the monkeys to reach their head with their arms by means of a 3D printed 'safety box' (designed using Autodesk Fusion 360), i.e. a nylon-12 surface that surrounded the animals' neck and thus kept the EEG cap and electrodes away from the animals' reach. Throughout the experiment, the monkey's head was restrained using a titanium headpost.

*Behavioral task and paradigm*

The task begun with the presentation of the target (an outlined grey circle, 2 DVA in diameter) placed in the center of the screen, together with the visual cursor (a white dot, 3 DVA diameter), placed below the target when no force was exerted on the isometric joystick (Fig. 1b). The monkey was required to bring the cursor inside the target, by exerting a force of 20N on the isometric joystick (on the y-axis, i.e. away from the body, Fig. 1a). The animal had to reach the target within 2 s from trial onset (i.e. presentation of the target), and keep the cursor within the target until the end of the trial (i.e. disappearance of the target). Trial duration ranged from 7 to 10 s (rectangular distribution). If the monkey did not reach the target within 2 s from its appearance or did not hold the cursor inside it for the whole trial duration, the trial was aborted. Otherwise, the trial was considered successful, and the animal received 1.75 ml of liquid reward (Fig. 1b).

*Experimental paradigm*

While holding the cursor within the target, monkeys experienced two types of trials. On 1/3 of the trials, an auditory stimulus was presented (1 m distance, frequency 3.3 kHz, duration 50 ms). These trials are hereafter called “Beep trials”. The stimulus was always presented at least 3 s after the cursor had entered the target and not later than 3 seconds before the target disappearance. Within this time range, the timing of the stimulus was randomly assigned. On the remaining 2/3 of the trials, no auditory stimuli were presented, and monkeys were required to hold the cursor within the target for a comparable amount of time. These trials are hereafter called “No-Beep trials”. Beep and No-Beep trials were presented in a randomized order, within mini-blocks of 6 trials (2 Beep and 4 No-Beep trials), with the only caveat that no more than 2 Beep trials could be presented consecutively across successive mini-blocks.

*EEG equipment and montage (Experiment 1)*

We recorded the electroencephalogram (EEG) using 29 active electrodes placed on the scalp (BioSemi Active-2 system). The data were sampled at 1024 Hz. The electrodes were mounted on two custom-made caps (http://www.easycap.de), tailored to fit each animal’s head, according to the layout displayed on Fig. 1c.

The BioSemi system replaces the ground electrodes with two electrodes named CMS (Common Mode Sense, active electrode) and DRL (Driven Right Leg, passive electrode). According to the system’s guidelines, CMS should (ideally) be placed in the centre of the measuring electrodes, while DRL should be placed relatively away from them. While placing CMS, we also had to consider the position of the headpost, being approximately over Cz in

monkey M, and over Cpz in monkey T. Therefore, CMS was placed on Cz (in monkey T) and on Cpz (in monkey M). DRL was always placed on frontal-left side of the animal's head (see the layout displayed on Fig. 1c, CMS and DRL are highlighted using grey dots).

*Intracortical recordings (Experiment 2)*

Neural raw signals were recorded from area BA9, using a 5-channel linear multiple-electrode array system for extracellular recording (Minimatrix 05. Thomas Recording, Germany). Inter-electrode distance was 0.3 mm. Each electrode (quartz-insulated platinum-tungsten fibers 80 mm diameter, 0.8–2.5 MOhm impedance) was guided through the intact dura into the cortical tissue (one specific recording site per session) through a remote controller. The raw neural signal was amplified, digitized at 24 kHz, and transmitted through optical fibers to a digital signal processing unit (RA16PA-RX5–2, Tucker-Davis Technologies) where it was stored.

*Data analysis (Experiment 1)*

In Experiment 1 we collected 327 successful Beep trials for monkey M (12 recording sessions, 27.25 ± 16.33 trials per session) and 365 successful Beep trials for monkey T (8 recording sessions, 45.62 ± 8.44 trials per session). These data were analysed by applying the same pipeline (described hereafter) to the two datasets (one for each monkey) separately. This approach was preferred over the alternative 'pooling' over the two datasets (Fries and Maris 2021) because the latencies of the force responses observed in the two animals were not always overlapping in time (see below).

*Force analysis.* Continuous force data were low-pass filtered (35 Hz, Butterworth, third order) and then segmented into epochs of 3 s. For Beep trials, the epochs started 0.4 s prior to stimulus onset and ended 2.6 s following it. For No-Beep trials, equally long epochs were extracted relatively to randomly-assigned time points comprised within the interval during which a stimulus could have been presented (i.e. at least 3 s after the cursor had entered into the target and not later than 3 s before the disappearance of the target). Force data comprised two channels $F_x$ and $F_y$ (associated with the force components exerted on the x and y axes of the transducer, respectively) and its magnitude F (which was computed using the following formula).

$$F = \sqrt{{F_x}^2 + {F_y}^2}$$

Trials contaminated by artifacts (i.e. deviating >4 SDs from the animal's mean exerted force F across all trials) were excluded from further analyses (Novembre et al. 2018, 2019). The corresponding EEG timeseries were also excluded. These trials constituted 3.01% (monkey T) and 4.28% (monkey M) of the total number of trials. Epochs were baseline corrected using the -0.05 to 0 s prestimulus interval (Novembre et al. 2018, 2019). Beep and No-Beep trials were compared using two-sample t-tests (one for each timepoint).

*EEG analysis.* Continuous EEG data were band-pass filtered (1-35 Hz, Butterworth, third order) and then segmented into Beep and No-Beep epochs of 5 s (-1.4 s to 3.6 s). Because the datasets contained several movement artifacts, data pre-processing was assisted by a validated algorithm for automatic artifact-correction: Artifact Subspace Reconstruction (ASR, threshold value = 5) (Kothe and Makeig 2013; Plechawska-Wojcik et al. 2018). ASR is an adaptive algorithm based on principal component analysis. It estimates clean portions of data

to determine thresholds that are later used to reject large-variance components. The use of ASR was preferred over conventional 'data cleaning' procedures because of its automaticity, implying lower computational time and lesser (potentially arbitrary) decision-making (Somervail et al. 2023). We note that we also compared the current results to those obtained following a traditional 'data cleaning' procedure, which yielded similar results at the cost of several trials being rejected.

Following ASR, the EEG epochs were cropped to match the force epochs (i.e. -0.4 to 2.6 s). Noisy or faulty electrodes were interpolated by replacing their voltage with the average voltage of the neighbouring electrodes. Data were re-referenced using a common average reference (Nunez and Srinivasan 2006). Artifacts due to eye blinks or eye movements were subtracted using a validated method based on an independent component analysis (Jung et al. 2000). In all datasets, independent components related to eye movements had a frontal scalp distribution. We also estimated the voltage at electrodes Cz and Cpz (used for CMS and for the headholder) by computing the average voltage of the neighbouring electrodes. Finally, the EEG epochs were baseline corrected using the -0.2 to 0 s prestimulus interval. Beep and No-Beep trials were compared using paired-sampled t-tests (one for each timepoint).

The trial-by-trial correlation between EEG and force magnitude (F) epochs was computed consistently with our previous work (Novembre et al. 2018, 2019). Specifically, we first smoothed the signals using a moving average (sliding window = 20 ms). The signals were then resampled to 250 Hz to reduce computation time. Finally, the trial-by-trial correlation coefficient (Spearman's r) was computed between EEG amplitude and force magnitude, for all possible pairs of time points between the interval -50 to 400 ms of the EEG time course (i.e., the interval encompassing all EEG modulations) and the interval -50 to 2000 ms of the force time course (i.e., the interval encompassing all force modulations). This resulted in 29

correlation matrixes (one for each EEG electrode). Significant correlations were thresholded by extracting clusters encompassing at least two consecutive significant timepoints ($p<0.05$) associated to at least two neighbouring electrodes.

*Data analysis (Experiment 2)*

In Experiment 2 we collected 393 successful Beep trials for monkey M (28 recording sessions, 14.04 ± 4.05 trials per session) and 339 successful Beep trials for monkey T (25 recording sessions, 13.56 ± 1.90 trials per session).

Behavioural data from Experiment 2 were analysed by applying the same pipeline described for Experiment 1. Trials contaminated by artifacts (i.e. deviating >4 SDs from the animal's mean exerted force F across all trials) were excluded from further analyses. The corresponding LFP timeseries were also excluded. These trials constituted 3.20% (monkey M) and 4.78% (monkey T) of the total number of trials.

Continuous extracellular LFP data were band-pass filtered (1-35 Hz, Butterworth, third order), polarity-inverted (for comparability with the EEG signal), and then segmented into Beep and No-Beep epochs of 5 s (-1.4 s to 3.6 s). LFP data were recorded from 5 electrodes, each with a single recording site. Within each recording session, a variable number of electrodes failed to penetrate the dura and did not reach the target cortical depth. These electrodes were considered 'non-active', and their corresponding LFP timeseries were excluded from the analyses [69 out of 140 (49.29%) for monkey M, and 15 out 125 (12.00%) for monkey T]. The remaining 'active' electrodes were classified as 'superficial' or 'deep' by applying a median split on the cortical depth from which recordings were taken.

The trial-by-trial correlation between LFP and force epochs was computed as in Experiment 1. Correlation matrixes were calculated by pooling all 'active' electrodes together or by pooling 'superficial' or 'deep' electrodes separately. Significant correlations were thresholded for significant time intervals ($p < 0.05$).

## Results

*Stimulus-induced Force modulations (Experiment 1)*

In both monkeys, auditory stimuli elicited a consistent biphasic modulation of force magnitude (F; Fig. 2a third row): an initial force decrease was followed by a force increase. This pattern was strongly evocative of that previously observed in humans (Novembre et al 2018; 2019), even though the latency of the current modulations was somehow inconsistent across animals and species, as we discuss below in more detail. Notably, when considering behavioural responses, a certain degree of both inter-individual and inter-species difference is to be expected, consequent to the presence of unique individual strategies and perceptual-motor styles (Vidal and Lacquaniti 2021).

T-tests comparing the exerted force across Beep and No-Beep trials (i.e. trials during which there was no auditory stimulus, see Methods) confirmed the across-trial consistency of the observed biphasic modulation of force magnitude, in each animal. To assist interpretability of these modulations with respect to their human equivalents, the initial force decrease and the following increase will be hereafter referred to as *d1* and *i2*, respectively.

The latency of the force modulation, particularly the initial *d1*, was slightly different across animals. In monkey T *d1* peaked at ~150 ms, while in monkey M it peaked at ~270 ms post-stimulus. In contrast, the subsequent *i2* was more similar across animals: it began ~400-450 ms post-stimulus and lasted nearly the whole trial duration. Notably, and paralleling human observations (Novembre et al 2018; 2019), in both animals *d1* had a more transient character, while *i2* was more tonic.

Examining the simultaneous modulations of force separately on the x and y axes (Fig. 2a, first and second row), we reconstructed the average cursor trajectory before and after the presentation of the auditory stimulus (Fig. 2b). In both monkeys, prior to stimulus presentation, the cursor slowly drifted towards the bottom of the screen (black arrow, Fig. 2b). Bearing in mind that a force resulting in an upward movement on the y axis had to be exerted to keep the cursor inside the target, this observation is consistent with the well-known fatigue effect in isometric force tasks [which we and others also observed in humans; (Nazir et al. 2017; Novembre et al. 2018)]. Immediately after stimulus onset, the first force decrease (*d1*) resulted in a transient enhancement of the above-described pre-stimulus drift (blue arrow, Fig. 2b). The subsequent force rebound (*i2*) moved the cursor in the opposite direction, bringing it above the pre-stimulus position (red arrow, Fig. 2b).

Comparing the direction of these motion trajectories across monkeys, we noticed that they were consistent along the vertical y axis, but somehow different along the horizontal x axis: in monkey T the cursor drifted towards the right side of the monitor, while in monkey M it drifted to the left. This difference is possibly explained by the different position of each monkey relative to the monitor (slightly on the right-side of monkey M and on the left-side of monkey

T; see *experimental setup*). Thus, the different drifting along the x axis might be trivially explained by the different hand and arm posture adopted by the two animals.

Figure 2 about here

*Stimulus-induced EEG modulations (Experiment 1)*

The EEG modulation elicited by the auditory stimuli is displayed on Figure 3. The modulation of EEG voltage consisted of a triphasic pattern including an early positivity (P30), a negativity (N70) and a second longer lasting positivity (P130). The negative-positive N70 and P130 complex constitutes the well-known vertex potential that can be measured in human and non-human primates (Bancaud et al. 1953; Neville and Foote 1984; Pineda et al. 1989; Mouraux and Iannetti 2009; Gil-Da-Costa et al. 2013; Milne et al. 2016)

Both latencies and topographies of these EEG modulations were remarkably consistent across animals. Specifically, the P30, which had central and frontal distribution, peaked at 35 and 30 ms post-stimulus in T and M, respectively. The N70 had broader and more posterior distribution over the scalp, and it peaked at 75 and 80 ms in T and M, respectively. Finally, the early part of the P130 exhibited a central-frontal topography, peaking at 120 and 130 ms in T and M, respectively. Notably, the P130 lasted longer than the previous P30 and N70, and its initial frontal topography changed slightly throughout time, to become more widespread and centrally distributed ~180-200 ms post stimulus, particularly in monkey M (Fig. 3b). The t-tests comparing the EEG voltages associated to Beep and No-Beep trials confirmed the high across-trial consistency of all the described components (Fig. 3a, bottom).

Notably, monkey T exhibited a mild slow-rising negativity anticipating the stimulus. This component is most likely a contingent negative variation (CNV) (Walter et al. 1964; Borda 1970).

Figure 3 about here

*Trial-by-trial correlation between force and EEG modulations (Experiment 1)*

The trial-by-trial correlation between force and EEG modulations revealed several interesting relationships, which are outlined in Figure 4.

First, both monkeys exhibited a robust correlation between the P130 EEG wave and the force increase *i2* (cluster A, Fig. 4). This implies that trials in which the P130 had large amplitude were also associated with a large force increase. It is also important to examine *where* across the scalp this correlation occurred [i.e. where trial-by-trial fluctuations of EEG amplitude were more strongly coupled with fluctuations of *i2* magnitude, see (Novembre et al. 2018)]. In both animals, this correlation was stronger over the right hemisphere, i.e. contralaterally to the (left) hand exerting the force (Fig. 4, inset). Remarkably, both the correlation between the positive vertex potential and the *i2*, and the topography of such correlation were similar to what we previously observed in humans (Novembre et al. 2018, 2019).

We also observed two additional relationships between EEG and force modulations that, however, were not consistent across the two animals (clusters B, Fig. 4). First, in monkey M, the amplitude of the N70 correlated negatively with the magnitude of the force increase

following *d1* (i.e. with the ascending branch of *d1* and the initial part of *i2*) – another result that parallels what we observed in humans (Novembre et al. 2018). Second, in monkey T, the amplitude of the CNV correlated negatively with the magnitude of *i2*.

Figure 4 about here

*Trial-by-trial correlation between force and LFP modulations*

Experiment 2 revealed a pattern of force modulation broadly similar to the one observed in Experiment 1 (compare Figs. 2 and 5). In both monkeys, auditory stimuli elicited modulations of the overall force magnitude (F) in a biphasic pattern composed of an initial force decrease (*d1*) followed by a force increase (*i2*). In monkey M, *d1* peaked at 148 ms post-stimulus, while *i2* peaked at 359 ms post-stimulus. In monkey T, *d1* showed a double peak (at 163 and 409 ms post-stimulus), due to an additional force increase peaking at 281 ms post-stimulus. The late force increase *i2* started ~400 ms post-stimulus and peaked >1 s post-stimulus. The morphology of these force responses, specifically that of the *i2,* was comparable to that described above (Figs. 2 and 5).

The auditory stimuli also elicited LFP modulations markedly similar to the EEG modulations described above (compare Experiment 1 and 2, Fig. 3 and 5). Specifically, these modulations entailed a triphasic pattern consisting of an early positivity (36 ms post-stimulus in both M and T), a negativity (78-79 ms in both M and T) and a second longer lasting positivity. In monkey M, this last positivity was very similar to what observed in Experiment 1 and peaked at 127 ms post-stimulus. In monkey T, this positive component appeared to be split into two halves (peaking at 106 and 215 ms post-stimulus, respectively), due to an additional negative

443 deflection peaking at 151 ms post-stimulus. Looking more closely to the results from
444 Experiment 1, this negativity embedded within the last P wave was also present in the EEG
445 data (Figs. 3 and 4, left), although less clearly than in the LFP data (Fig. 5).

446

447 Most compellingly, the correlation between LFP and Force data was extremely similar to that
448 observed between EEG and Force (compare Figs. 4 and 5). Specifically, the late positivity
449 evoked by the auditory stimulus correlated, on a trial-by-trial level, with the late force increase
450 *i2*, in both animals (Cluster A, Fig. 5). When we looked at this correlation as a function of
451 cortical depth, i.e. considering selectively deep and superficial recording sites, we found that
452 the correlation between LFP and Force was clearer for deep electrodes (Fig. 6).

453

454 Figure 5 and 6 about here

455

456

## Discussion

In this study we investigated (1) whether the CMR – a multiphasic modulation of isometric force elicited by salient sensory stimuli – is present in non-human primates, and (2) its neural correlates. In the next sections we compare the CMR observed in monkeys and humans, and describe the neural responses elicited by the stimuli causing the CMR in monkeys, with particular emphasis on their tight coupling.

### *Force modulations: CMR in rhesus monkeys?*

In humans, sudden stimuli evoke a complex modulation of constantly-applied isometric force (CMR; Novembre et al. 2018, 2019; Somervail et al. 2021). An initial force decrease at 100 ms post-stimulus (*d1*) is followed by two force increases: one peaking at 250 ms post-stimulus (*i1*) and the other starting at ~350 ms and lasting for nearly 2 seconds (*i2*) (see Fig. 7). The current experiments show that monkeys exhibit force modulations reminiscent of the human CMR, with some differences that we discuss in detail. We particularly focus on the force increase, because of its (1) reproducibility across animals and experiments, and (2) tight correlation with electrocortical activity.

In both humans and monkeys, salient stimuli evoked an initial force decrease, followed by a force increase. However, while in humans we were able to distinguish two distinct force increases, this was mostly not the case in monkeys (Fig. 7): either they show only one increase (*i2*), or this difference is consequent to holding a joystick using the whole hand (power grip) rather than a transducer between the index and the thumb (i.e. a precision grip; Fig. 7).

The *i2* observed in monkeys started ~300-400ms post-stimulus and lasted 1s (monkey T) and 1.5s (monkey M), remarkably similar to the human *i2* (onset: ~350ms, duration: ~2s (Fig. 7)). Because of this similarity, we labelled the monkey force increase as *i2*. The human *i1* (onset: 250ms, duration: 200ms, Fig.7) does not have an homologous in monkeys in the context of the current task.

To study the functional significance of the monkey CMR, we reconstructed the cursor trajectory and made several intriguing observations that might clarify the function of *d1* and *i2* (Fig. 2). The downward cursor drift before stimulus likely reflects the well-known isometric force fatigue (Nazir et al. 2017; Novembre et al. 2018). Therefore, *d1* could be a further transient reduction of the tonic corticospinal output subserving task execution. Similarly, *i2* could be a corrective rebound, bringing the cursor back to its original pre-stimulus position, but overshooting: cursor position at the end of *i2* (red dots, Fig. 2) is higher than 400 ms before stimulus onset (black dots, Fig. 2). This is consistent with the idea that the CMR is a both reactive and adaptive behavior (RAB; Novembre and Iannetti 2021).

Figure 7 about here

*EEG/LFP modulations: the Vertex Potential in rhesus monkeys*

Sudden auditory stimuli evoked transient modulations of both EEG and LFP recordings, highly consistent within- and across-animals (Figs. 3,4,5). An early positivity (P30) was followed by a negativity (N70) and a final positivity (P130), consistent with previous recordings (Gil-Da-Costa et al. 2013; Milne et al. 2016; Neville and Foote 1984; Pineda et al. 1989).

Sudden auditory stimuli evoke a similar triphasic pattern in humans, although with longer latencies (P50-N100-P200). The latter two components, often labelled N1 and P2, constitute the widely-studied 'vertex potential', which indexes 'surprise' in response to isolated stimuli regardless of their sensory modality (Bancaud et al. 1953; Mouraux and Iannetti 2009; Somervail et al. 2021). The EEG/LFP responses in monkeys are highly reminiscent of the human vertex potential, with the shorter latencies explained by the shorter fiber tracts in macaques (Ringo et al. 1994; Caminiti et al. 2009; Woodman 2012). Notably, despite the coupling with motor behavior (further discussed below), the vertex potential should not be confused with other ERPs classically associated with action preparation such as the lateralized readiness potential (LRP). Indeed, the LRP is constituted by a single monophasic component, with different topography and timescale, besides being elicited in different experimental paradigms (Kornhuber and Deecke 1965; Vaughan et al. 1968).

Despite the thick muscles surrounding the ears and neck of macaques (Woodman 2012) we obtained remarkably neat EEG topographies, extremely similar to those observed in humans (Mouraux and Iannetti 2009; Luck 2014). By combining well-established with recently-developed EEG denoising algorithms (independent component analysis and artifact subspace reconstruction (Jung et al. 2000; Kothe and Makeig 2013; Plechawska-Wojcik et al. 2018) we provide one of the most comprehensive characterizations of event-related potentials in awake monkeys (Fig. 3).

*Neurophysiology of the CMR*

Second objective of this study was to investigate the neurophysiology of the CMR. In humans the CMR modulations are tightly coupled to the electro-cortical responses elicited by the same sudden and unexpected stimuli (Novembre et al. 2018, 2019): the trial-by-trial amplitude of

both the negative and positive vertex potential waves (N100, P200) strongly predicts the magnitude of CMR force increases. Here we show a similar coupling in monkeys (Fig. 7).

The P130 in EEG/LFP (equivalent to the human P200) was positively trial-by-trial correlated with the force *i2,* in both animals (clusters A, Figs. 4,5). It is worth noting that while the P130 scalp distribution was symmetrical (Fig. 3b), the scalp distribution of this correlation had a hint of lateralization towards the hemisphere contralateral to the hand exerting the force (Fig. 4, insets). This suggestion of a discrepancy between voltage and correlation topographies, together with the clearer dissociation previously observed in humans (Novembre et al. 2018), suggests that corticospinal projections originating in the frontal cortex contralateral to the hand performing the task might be modulated by the vertex potential. This possibility is not conclusive, and we refer to Novembre et al. 2018 for a discussion on the possible existence of a third structure modulating both the vertex potential and the motor cortex producing the CMR. Still, the possibility of a cortical origin of the CMR cannot be ruled out especially when considering that LFPs were measured from the right dorsolateral prefrontal cortex contralateral to the limb performing the task (Figs. 1,5). Thus, EEG/force and LFP/force correlations in monkeys replicate and extend human observations, providing strong evidence that cortical and muscular responses elicited by sudden and unexpected environmental events are strongly coupled.

Other correlations should be interpreted with caution, as they were inconsistent across animals, although sometimes consistent with human results (clusters B, Figs. 4,7). Consistently with human results, in monkey M the trial-by-trial amplitude of the N70 (homologous of the human N100) correlated negatively with the *i2* magnitude: a larger N70 predicted a stronger subsequent *i2*. Observing the N70-*i2* correlation in one animal and the P130-*i2* correlation in both animals is consistent with the less robust N100-*i2* correlation

559 ($p$=0.019) and the stronger P200-*i2* correlation ($p$<0.001) in humans (Novembre et al. 2018).
560 Unexpectedly, in monkey T the CNV amplitude correlated negatively with the *i2* magnitude.
561 Given that this result was observed only in one animal, and that several equally-valid post-hoc
562 explanations could be put forward, we prefer to be cautious and report it without providing
563 potentially-incorrect interpretations.

564

565 Given that we only used correlational techniques, it is difficult to identify the circuits potentially
566 mediating the CMR. We recorded from BA9, a high-order associative region shown to control
567 hand force in both monkeys and humans (Ehrsson et al. 2000; Vaillancourt et al. 2007; Badoud
568 et al. 2017). Unilateral lesioning BAs 9/10 impairs hand force control, leaving other motor
569 behaviors intact. Human studies have shown that this area is part of a network subserving grip
570 force control (Ehrsson et al. 2000, 2001; Vaillancourt et al. 2007; Neely et al. 2013), important
571 for real-time monitoring of force control accuracy, taking into account sensory feedback
572 (Ehrsson et al. 2001; Neely et al. 2013). These observations and our results make BA9 a
573 suitable candidate region mediating the CMR. Notably, other RABs (online motor correction,
574 action stopping) have been associated to dlPFC activity (Cisek 2007; Scott 2012; Wessel and
575 Aron 2017; Novembre and Iannetti 2021). The role of BA9 might unify these distinct lines of
576 research, and suggest a unified neural network mediating fast modulations of motor output in
577 response to sudden environmental stimuli (Novembre and Iannetti 2021). Still, whether and
578 through which pathway BA9 might influence the motor output and lead to the observed force
579 modulations remains an open question to be addressed in future studies using causal
580 approaches.

581

582 Furthermore, it is important to highlight that recording from a single area limits result
583 interpretability, particularly given that sudden stimuli activate large and widespread cortical
584 territories (Fig. 3; Mouraux and Iannetti 2009; Liang et al. 2010). We cannot therefore

exclude that BA9 does not specifically modulate the motor output, and that other cortical areas would show similar LFP responses and correlation with CMR components. Studies entailing multiple intraparenchymal recordings will be necessary to test this likely alternative possibility.

591 **References**

592


593 Badoud S, Borgognon S, Cottet J, Chatagny P, Moret V, Fregosi M, Kaeser M, Fortis E,
594 Schmidlin E, Bloch J, Brunet JF, Rouiller EM. 2017. Effects of dorsolateral prefrontal
595 cortex lesion on motor habit and performance assessed with manual grasping and
596 control of force in macaque monkeys. Brain Struct Funct. 222:1193–1206.

597 Bancaud J, Bloch V, Paillard J. 1953. Contribution EEG a letude des potentiels evoques
598 chez lhomme au niveau du vertex. Rev Neurol (Paris). 89:399–418.

599 Battaglia-Mayer A, Buiatti T, Caminiti R, Ferraina S, Lacquaniti F, Shallice T. 2014.
600 Correction and suppression of reaching movements in the cerebral cortex:
601 Physiological and neuropsychological aspects. Neurosci Biobehav Rev. 42:232–251.

602 Battaglia-Mayer A, Ferrari-Toniolo S, Visco-Comandini F, Archambault PS, Saberi-
603 Moghadam S, Caminiti R. 2013. Impairment of online control of hand and eye
604 movements in a monkey model of optic ataxia. Cereb Cortex. 23:2644–2656.

605 Boehler CN, Münte TF, Krebs RM, Heinze HJ, Schoenfeld MA, Hopf JM. 2009. Sensory
606 MEG responses predict successful and failed inhibition in a stop-signal task. Cereb
607 Cortex. 19:134–145.

608 Borda RP. 1970. The effect of altered drive states on the contigent negative variation (CNV)
609 in rhesus monkeys. Electroencephalogr Clin Neurophysiol. 29:173–180.

610 Caminiti R, Ghaziri H, Galuske R, Hof PR, Innocenti GM. 2009. Evolution amplified
611 processing with temporally dispersed slow neuronal connectivity in primates. Proc Natl
612 Acad Sci U S A. 106:19551–19556.

613 Cisek P. 2007. Cortical mechanisms of action selection: The affordance competition
614 hypothesis. Philos Trans R Soc B Biol Sci. 362:1585–1599.

615 Corneil BD, Munoz DP, Chapman BB, Admans T, Cushing SL. 2008. Neuromuscular
616 consequences of reflexive covert orienting. Nat Neurosci. 11:13–15.

617 Corneil BD, Olivier E, Munoz DP. 2004. Visual responses on neck muscles reveal selective
618 gating that prevents express saccades. Neuron. 42:831–841.

619 Ehrsson HH, Fagergren A, Forssberg H. 2001. Differential fronto-parietal activation
620 depending on force used in a precision grip task: An fMRI study. J Neurophysiol.
621 85:2613–2623.

622 Ehrsson HH, Fagergren A, Jonsson T, Westling G, Johansson RS, Forssberg H. 2000.
623 Cortical activity in precision- versus power-grip tasks: An fMRI study. J Neurophysiol.
624 83:528–536.

625 Engbert R, Kliegl R. 2003. Microsaccades uncover the orientation of covert attention. Vision
626 Res. 43:1035–1045.

627 Ferrari-Toniolo S, Visco-Comandini F, Battaglia-Mayer A. 2019. Two brains in action: Joint-
628 action coding in the primate frontal cortex. J Neurosci. 1512–1518.

629 Ferrari-Toniolo S, Visco-Comandini F, Papazachariadis O, Caminiti R, Battaglia-Mayer A.
630 2015. Posterior Parietal Cortex Encoding of Dynamic Hand Force Underlying Hand-
631 Object Interaction. J Neurosci. 35:10899–10910.

632 Fries P, Maris E. 2021. What to do if N is two? arXiv:210614562.

633 Giarrocco F, Bardella G, Giamundo M, Fabbrini F, Brunamonti E, Pani P, Ferraina S. 2021.
634 Neuronal dynamics of signal selective motor plan cancellation in the macaque dorsal
635 premotor cortex. Cortex. 135:326–340.

636 Gil-Da-Costa R, Stoner GR, Fung R, Albright TD. 2013. Nonhuman primate model of
637 schizophrenia using a noninvasive EEG method. Proc Natl Acad Sci U S A.
638 110:15425–15430.

639 Goonetilleke SC, Katz L, Wood DK, Gu C, Huk AC, Corneil BD. 2015. Cross-species
640 comparison of anticipatory and stimulus-driven neck muscle activity well before
641 saccadic gaze shifts in humans and nonhuman primates. J Neurophysiol. 114:902–913.

642 Jung TP, Makeig S, Westerfield M, Townsend J, Courchesne E, Sejnowski TJ. 2000.
643 Removal of eye activity artifacts from visual event-related potentials in normal and
644 clinical subjects. Clin Neurophysiol. 111:1745–1758.

645 Kornhuber HH, Deecke L. 1965. [CHANGES IN THE BRAIN POTENTIAL IN VOLUNTARY
646 MOVEMENTS AND PASSIVE MOVEMENTS IN MAN: READINESS POTENTIAL AND
647 REAFFERENT POTENTIALS]. Pflugers Arch Gesamte Physiol Menschen Tiere.
648 284:1–17.

649 Kothe CA, Makeig S. 2013. BCILAB: A platform for brain-computer interface development. J
650 Neural Eng. 10.

651 Lee RG, Tatton WG. 1975. Motor Responses to Sudden Limb Displacements in Primates
652 with Specific CNS Lesions and in Human Patients with Motor System Disorders. Can J
653 Neurol Sci / J Can des Sci Neurol. 2:285–293.

654 Liang M, Mouraux a., Chan V, Blakemore C, Iannetti GD. 2010. Functional characterisation
655 of sensory ERPs using probabilistic ICA: Effect of stimulus modality and stimulus
656 location. Clin Neurophysiol. 121:577–587.

657 Luck SJ. 2014. An Introduction to the Event-Related Potential Technique. MIT press.

658 Menon V, Uddin LQ. 2010. Saliency, switching, attention and control: a network model of
659 insula function. Brain Struct Funct. 214:655–667.

660 Milne AE, Mueller JL, Männel C, Attaheri A, Friederici AD, Petkov CI. 2016. Evolutionary
661 origins of non-adjacent sequence processing in primate brain potentials. Sci Rep. 6:1–
662 10.

663 Mouraux A, Iannetti GD. 2009. Nociceptive laser-evoked brain potentials do not reflect

664 nociceptive-specific neural activity. J Neurophysiol. 101:3258–3269.

665 Näätänen R, Paavilainen P, Rinne T, Alho K. 2007. The mismatch negativity ( MMN ) in
666 basic research of central auditory processing : A review. Clin Neurophysiol. 118:2544–
667 2590.

668 Nazir TA, Hrycyk L, Moreau Q, Frak V, Cheylus A, Ott L, Lindemann O, Fischer MH,
669 Paulignan Y, Delevoye-Turrell Y. 2017. A simple technique to study embodied
670 language processes: the grip force sensor. Behav Res Methods. 49:61–73.

671 Neely KA, Coombes SA, Planetta PJ, Vaillancourt DE. 2013. Segregated and overlapping
672 neural circuits exist for the production of static and dynamic precision grip force. Hum
673 Brain Mapp. 34:698–712.

674 Neumann O. 1990. Direct parameter specification and the concept of perception. Psychol
675 Res. 52:207–215.

676 Neville HJ, Foote SL. 1984. Auditory event-related potentials in the squirrel monkey:
677 Parallels to human late wave responses. Brain Res. 298:107–116.

678 Novembre G, Iannetti GD. 2021. Towards a unified neural mechanism for reactive adaptive
679 behaviour. Prog Neurobiol. 204:102115.

680 Novembre G, Pawar V, Bufacchi R, Kilintari M, Srinivasan M, Rothwell J, Haggard P, Iannetti
681 G. 2018. Saliency detection as a reactive process: unexpected sensory events evoke
682 cortico-muscular coupling. J Neurosci. 38:2474–17.

683 Novembre G, Pawar VM, Kilintari M, Bufacchi RJ, Guo Y, Rothwell JC, Iannetti GD. 2019.
684 The effect of salient stimuli on neural oscillations, isometric force, and their coupling.
685 Neuroimage. 198.

686 Nunez PL, Srinivasan R. 2006. Electric fields of the brain: the neurophysics of EEG. Oxford
687 University Press.

688 Picton TW. 1992. The P300 Wave of the Human Event-Related Potential. J Clin
689 Neurophysiol. 9:456–479.

690 Pineda JA, Foote SL, Neville HJ. 1989. Effects of locus coeruleus lesions on auditory, long-
691 latency, event-related potentials in monkey. J Neurosci. 9:81–93.

692 Plechawska-Wojcik M, Kaczorowska M, Zapala D. 2018. The Artifact Subspace
693 Reconstruction (ASR) for EEG Signal Correction. A Comparative Study.

694 Pruszynski JA, King GL, Boisse L, Scott SH, Flanagan JR, Munoz DP. 2010. Stimulus-
695 locked responses on human arm muscles reveal a rapid neural pathway linking visual
696 input to arm motor output. Eur J Neurosci. 32:1049–1057.

697 Rangel BO, Novembre G, Wessel JR. 2023. Measuring the nonselective effects of motor
698 inhibition using isometric force recordings. Behav Res Methods. 2022.11.17.516968.

699 Ringo JL, Doty RW, Demeter S, Simard PY. 1994. Time is of the essence: a conjecture that
700 hemispheric specialization arises from interhemispheric conduction delay. Cereb
701 Cortex. 4:331–343.

702 Satta E, Ferrari-Toniolo S, Visco-Comandini F, Caminiti R, Battaglia-Mayer A. 2017.
703 Development of motor coordination during joint action in mid-childhood.
704 Neuropsychologia. 105:111–122.

705 Schevernels H, Bombeke K, Borght L Van Der, Hopf J, Krebs RM, Boehler CN. 2015.
706 NeuroImage Electrophysiological evidence for the involvement of proactive and reactive
707 control in a rewarded stop-signal task. Neuroimage. 121:115–125.

708 Scott SH. 2012. The computational and neural basis of voluntary motor control and planning.
709 Trends Cogn Sci. 16:541–549.

710 Scott SH. 2016. A Functional Taxonomy of Bottom-Up Sensory Feedback Processing for
711 Motor Actions. Trends Neurosci. 39:512–526.

712 Sokolov EN. 1963. Higher nervous functions: the orienting reflex. Annu Rev Physiol. 25:545–
713 580.

714 Somervail R, Bufacchi RJ, Salvatori C, Neary-Zajiczek L, Guo Y, Novembre G, Iannetti GD.
715 2021. Brain Responses to Surprising Stimulus Offsets: Phenomenology and Functional
716 Significance. Cereb Cortex. 1–14.

717 Somervail R, Cataldi J, Stephan AM, Siclari F, Iannetti GD. 2023. Dusk2Dawn: an EEGLAB
718 plugin for automatic cleaning of whole-night sleep electroencephalogram using Artifact
719 Subspace Reconstruction. Sleep.

720 Vaillancourt DE, Yu H, Mayka MA, Corcos DM. 2007. Role of the basal ganglia and frontal
721 cortex in selecting and producing internally guided force pulses. Neuroimage. 36:793–
722 803.

723 Vaughan HG, Costa LD, Ritter W. 1968. Topography of the human motor potential.
724 Electroencephalogr Clin Neurophysiol. 25:1–10.

725 Vidal PP, Lacquaniti F. 2021. Perceptual - motor styles. Exp Brain Res.

726 Walter WG. 1964. the Convergence and Interaction of Visual, Auditory, and Tactile
727 Responses in Human Nonspecific Cortex. Ann N Y Acad Sci. 112:320–361.

728 Walter WG, Cooper R, Aldrige VJ, Mccallum WC, Winter AL. 1964. Contingent Negative
729 Variation : An Electric Sign of Sensori-Motor Association and Expectancy in the Human
730 Brain. Nature. 203:380–384.

731 Wessel JR, Aron AR. 2017. On the globality of motor suppression : unexpected events and
732 their influence on behavior and cognition. Neuron. 93:259–280.

733 Woodman GF. 2012. Homologues of Human ERP Components in Nonhuman Primates, The
734 Oxford Handbook of Event-Related Potential Components.

735

## Figure Legends

**Figure 1**. Experimental materials and methods. (A) Experimental paradigm. Two macaques were trained to exert a force on an isometric joystick using the left hand. The force applied on the x and y axes of the joystick was used to control the position of a cursor moving on a monitor. During a period of static force application, sudden task-irrelevant auditory stimuli were delivered through a beeper placed behind the monitor. (B) Task timeline. The task begun with presentation of the target on the center of the screen. Monkeys had 2 seconds to bring the cursor (white dot) inside the target (white circle) and were required to hold the cursor there for a variable time interval (ranging between 7 and 10 seconds). In 33% of the trials, auditory stimuli were unexpectedly delivered during this interval. If the cursor remained inside the target, the trial was considered successful, and a liquid reward was given. Trials were separated by a 2-2.5 second (jittered) interval (during which monkeys were not required to exert force and therefore the cursor was likely to be back to the start position). (C) EEG and LFP recording. In Experiment 1, we recorded EEG signals using 29 active electrodes (black dots) and 2 "zero-reference" electrodes (grey dots), mounted on custom-made EEG caps tailored to fit each animal's head. In Experiment 2, local field potentials (LFP) were recorded from the right dorso-lateral prefrontal cortex (Brodmann area 9), through a 5-channel multiple-electrode array system for extracellular recording.

**Figure 2**. Stimulus-induced Force modulations. A: Stimulus-induced modulations of force magnitude over the x (first row) and y (second row) axes. A composite index of force (F), representing the overall force magnitude regardless of its x-y directionality, is displayed in the third row. The coloured background represents t values yielded after comparing Beep (black line) and No-Beep (grey line) trials. B: Illustrative representation

of the position of the cursor (dot) with respect to the target (circle) over time, at four different time points: baseline onset (black), stimulus presentation (grey), peak of force decrease (blue) and peak of force increase (red). The density maps represent all positions held by the dot over the course of all trials.

**Figure 3**. Stimulus-induced EEG modulations. A (top): Single-trial modulations (at electrode Cz). Trials are sorted by their order of occurrence. The coloured background represents amplitude. (bottom): across-trial averages of EEG modulations (at electrode Cz). The coloured background represents t values yielded after comparing Beep (black line) and No-Beep (grey line) trials. B: EEG topographies of the main modulations. Time points of each topography are marked with vertical grey lines crossing the EEG average waveform (shown in panel A, bottom).

**Figure 4**. Trial-by-trial correlation between force and EEG modulations. Trial-by-trial correlations between stimulus-induced force and EEG modulations. Bidimensional plots represent the significant trial-by-trial correlation coefficients (cluster-corrected Spearman's r) between EEG and force, for all possible pairs of time points, at electrode Cz. The topographies of the main correlation clusters are also plotted. The EEG timeseries (plotted vertically) and the force timeseries (plotted horizontally) are shown to assist interpretability of the correlations. Note that the correlation between the EEG positive wave (P130) and the force increase (i2) is slightly lateralized towards the right scalp regions, i.e. contralateral to the (left) arm that exerted the force.

**Figure 5**. Trial-by-trial correlation between force and LFP modulations. Trial-by-trial correlations between stimulus-induced force and LFP modulations (recorded from the dorso-lateral Prefrontal Cortex, dlPFC). The bidimensional plots represent the

significant trial-by-trial correlation coefficients (cluster-corrected Spearman's r) between LFP and force, for all possible pairs of time points (pooling all 'active' electrodes). The LFP timeseries (plotted vertically) and the force timeseries (plotted horizontally) are shown to assist interpretability of the correlations. The correlation between the LFP positive wave (equivalent to the EEG P130) and the force increase (i2) is highlighted.

**Figure 6**. Trial-by-trial correlations between stimulus-induced force and LFP modulations at different cortical depths. The bidimensional plots represent the significant trial-by-trial correlation coefficients (cluster-corrected Spearman's r) between LFP and force for all possible pairs of time points, for either superficial (A) or deep (B) recording sites. The LFP timeseries (plotted vertically) and the force timeseries (plotted horizontally) are shown to assist interpretability of the correlations. The correlation between the LFP positive wave (equivalent to the EEG P130) and the force increase (i2) is highlighted. Note the clearer LFP-force correlations in deep recording sites.

**Figure 7**. Comparison of stimulus-induced EEG-force correlations in monkeys and humans. Data are from the current study (Monkey M, left) and from Novembre et al., 2018 (28 human participants, right). The bidimensional plots represent the significant trial-by-trial correlation coefficients (cluster-corrected Spearman's r [monkey, left], and t-values comparing participants' Pearson's r [human, right]) between EEG and force for all possible pairs of time points, at electrode Cz (topographies of the highlighted clusters are plotted). The EEG timeseries (plotted vertically) and the force timeseries (plotted horizontally) are shown to assist interpretability of the correlations. Note that the correlation between the positive vertex wave (occurring earlier in monkeys [P130] than in humans [P250]) and the force increase (i2) is slightly lateralized towards the scalp regions contralateral to the hand that exerted the force (left hand in monkeys; right

814 hand in human participants). Note that the two datasets were re-referenced differently,
815 likely explaining the more focal (monkey) and global (human) topographies.
816

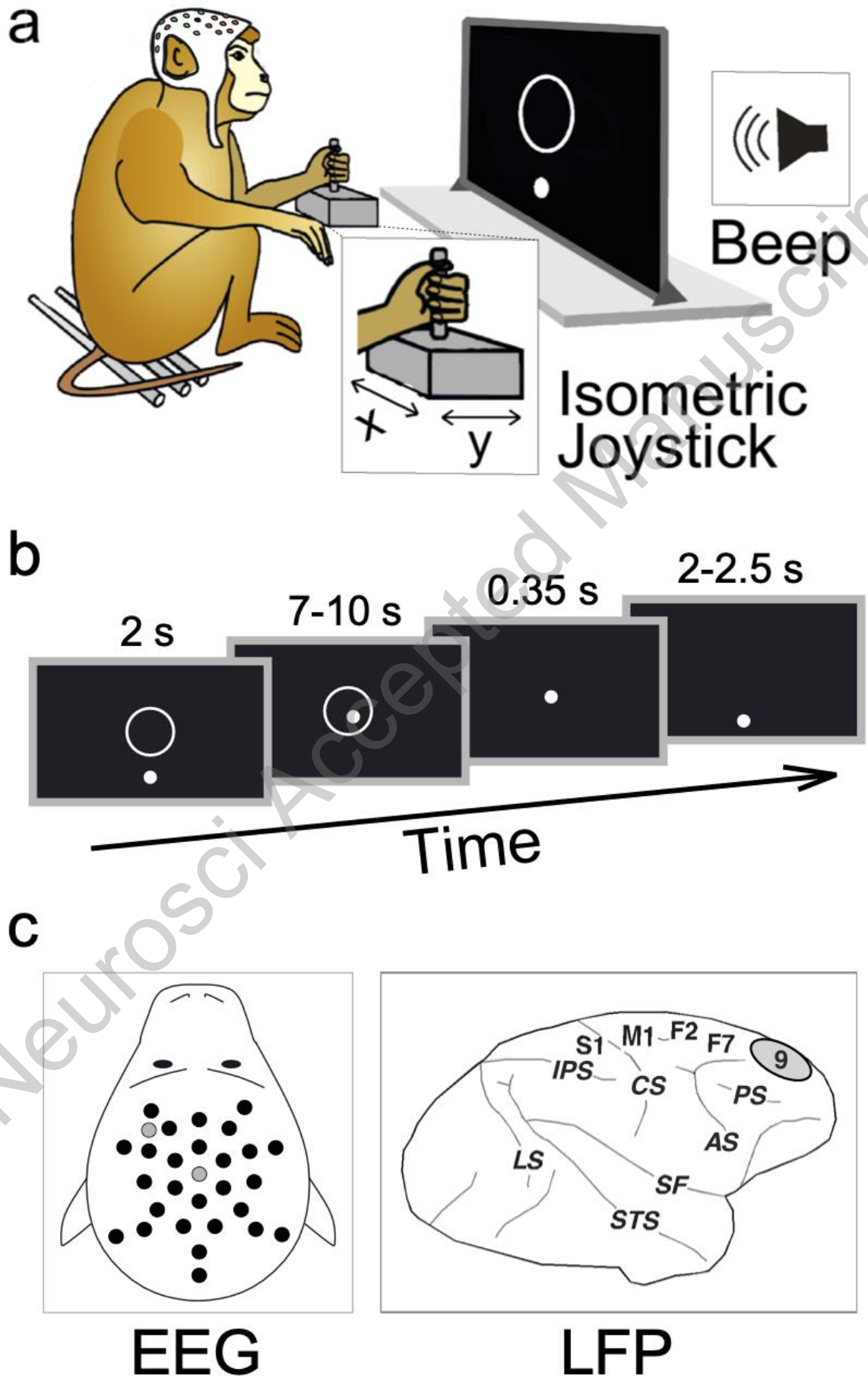


817

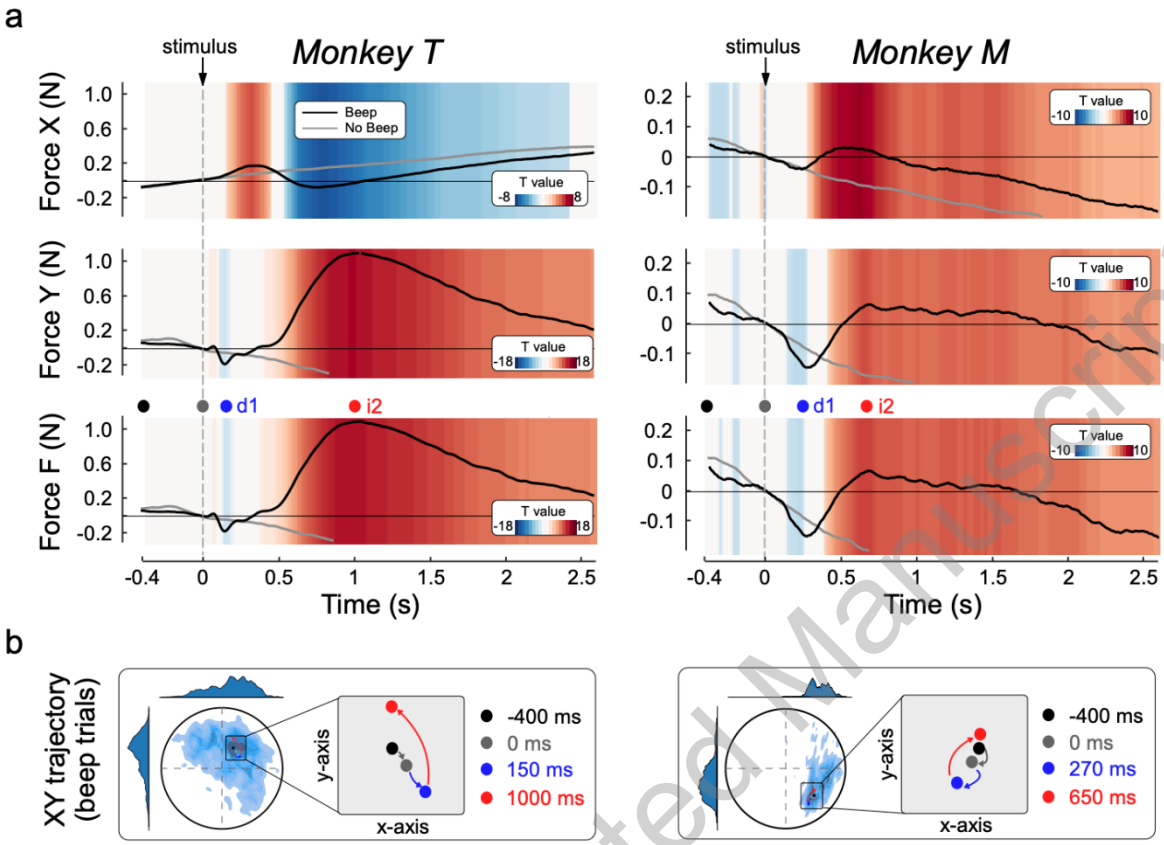


818

819

820

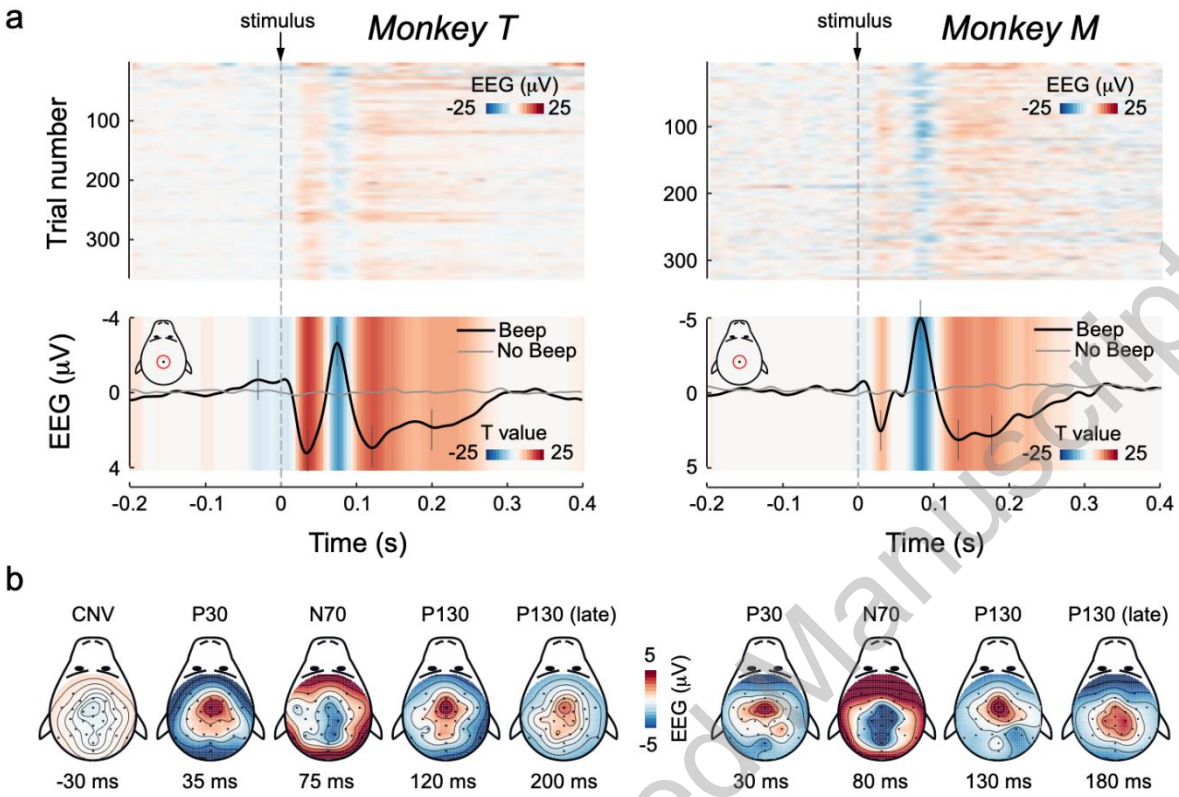


821

822

823

824

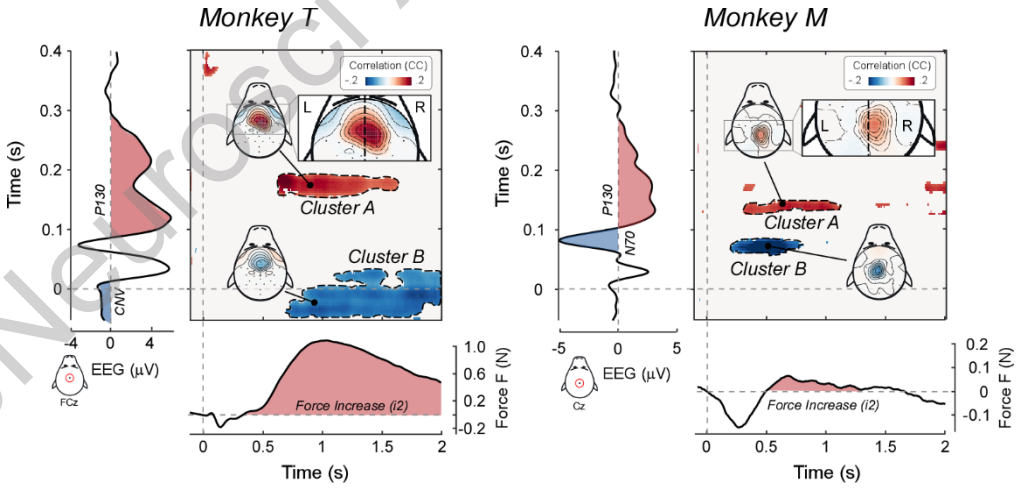


825

826

827

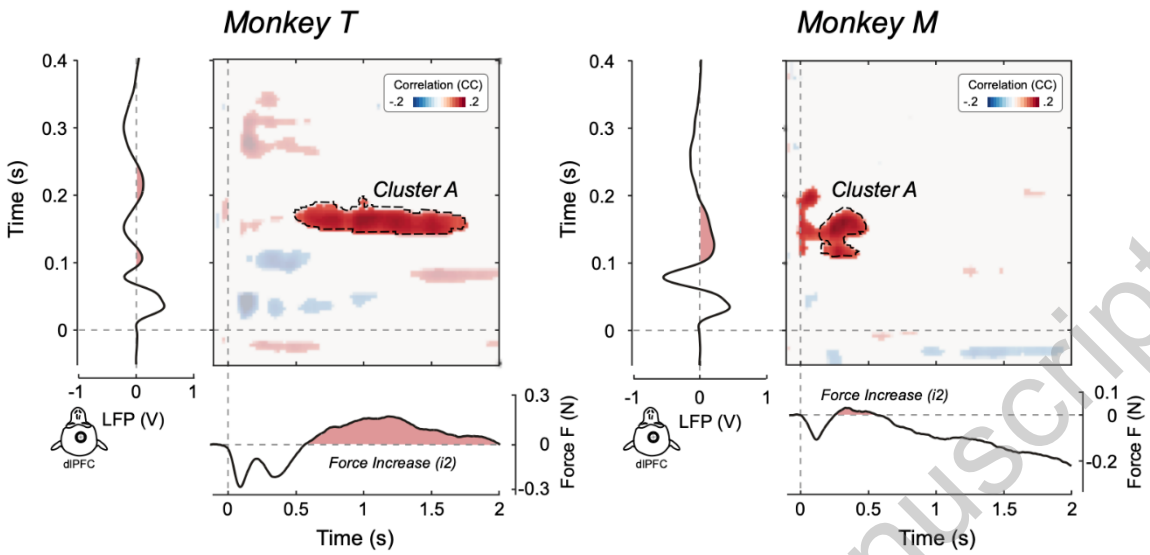


828

829

830

831

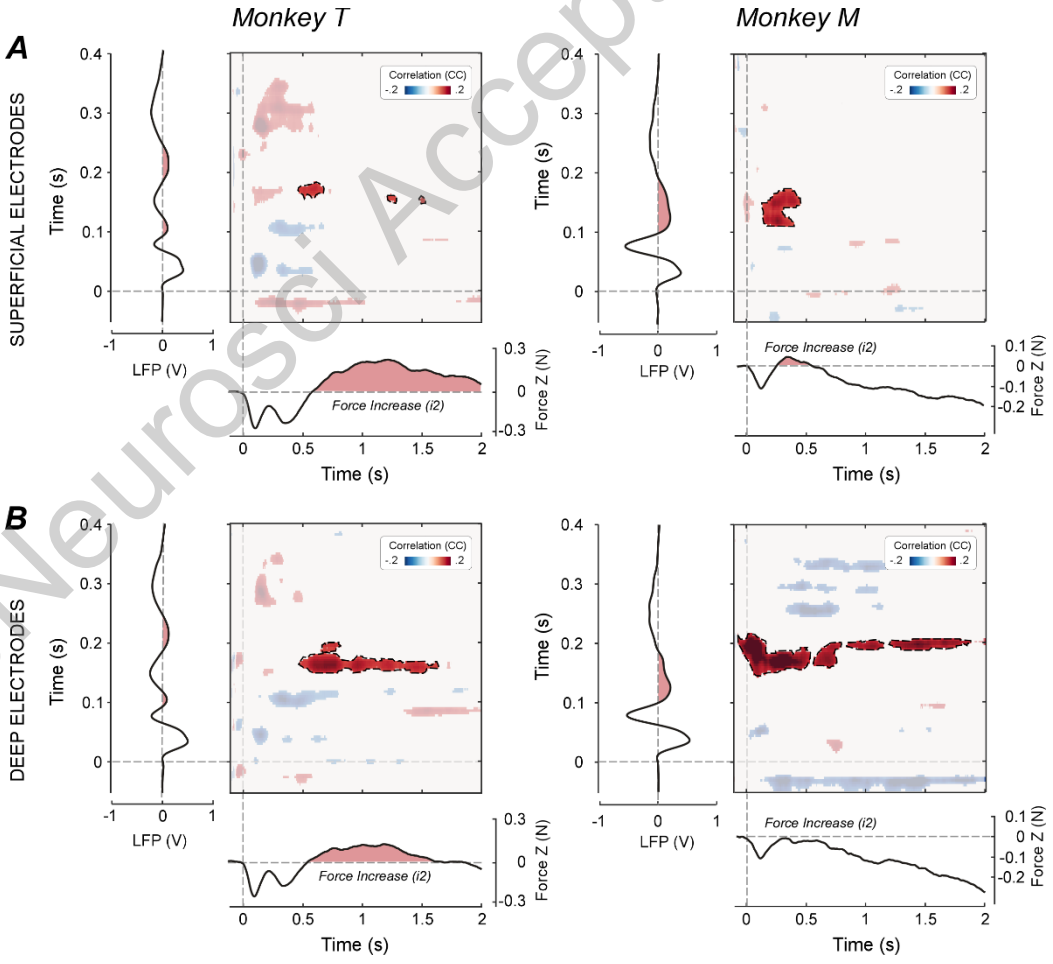


832

833

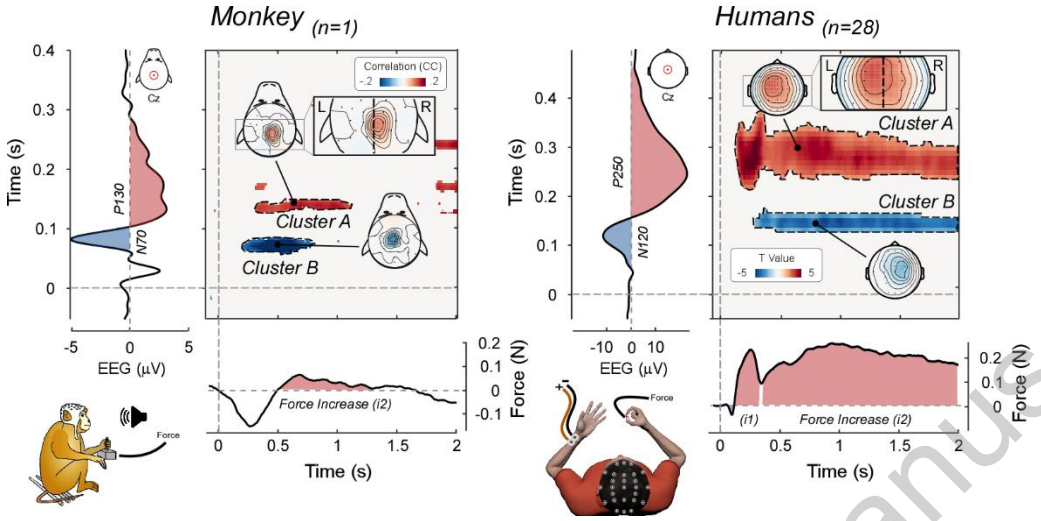


834